Supplementary information to:

Projection-biased dopamine neuron subpopulations coordinate immediate and future-oriented motivation

Hideyuki Matsumoto[1,2,*], Kenji Mizuseki[1,2,*]

[1]Department of Physiology, Osaka Metropolitan University Graduate School of Medicine, Osaka, 545-8585, Japan

[2]Department of Physiology, Osaka City University Graduate School of Medicine, Osaka, 545-8585, Japan

* Correspondence: matsumoto.hideyuki@omu.ac.jp, mizuseki.kenji@omu.ac.jp

This file contains:

1. Supplementary figures and figure legends (1–12)
2. References (in this file)

Unless otherwise noted, box plots in the supplementary figures show the median, interquartile range (IQR), and whiskers extending to the most extreme data points within 1.5 × IQR.

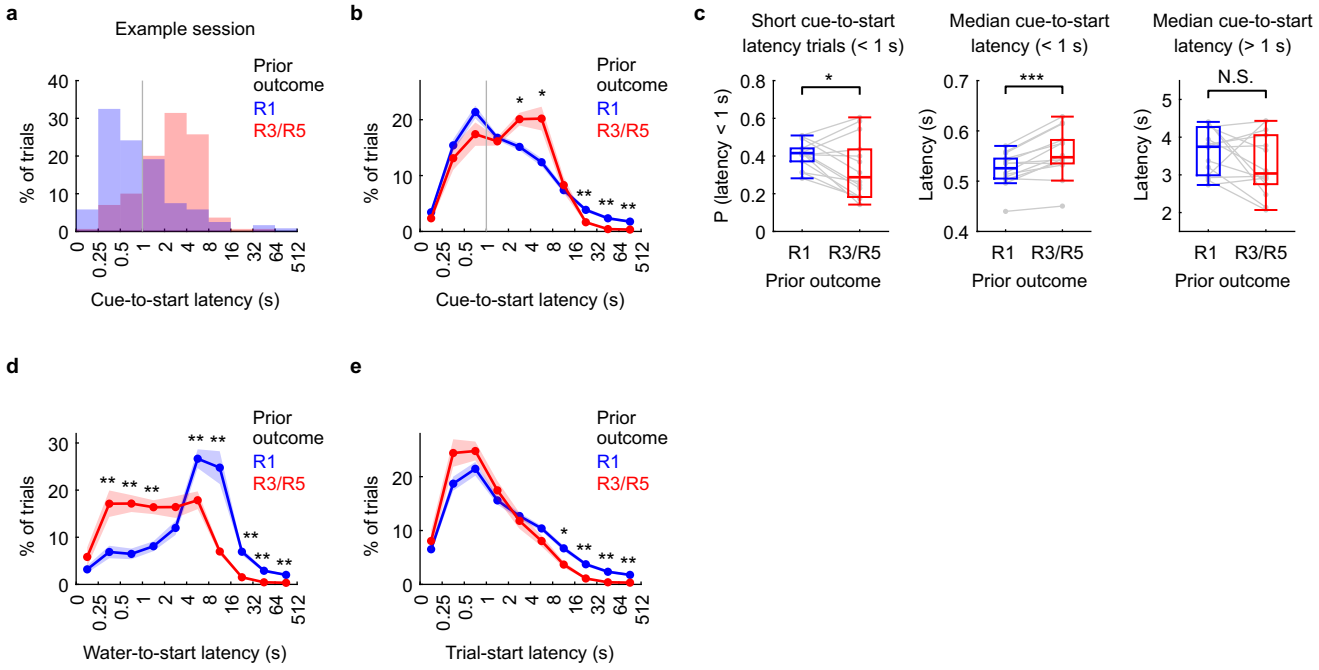

Supplementary Fig. 1 | Latency measures related to next-trial initiation as a function of prior outcome.

Cue-to-start, water-to-start, and trial-start latency distributions were compared across prior reward conditions. Distributions were plotted in 10 bins spaced on a $\log_2$ scale, with the first bin covering 0–0.25 s and subsequent bins spanning 0.25–512 s. In all panels, trials were grouped by prior outcome, defined as the reward delivered on the rewarded trial immediately preceding the measured latency: R1 (pooled across R1b and R1s) versus R3/R5 (pooled across R3 and R5).

a, Representative session showing the distribution (% of trials) of cue-to-start latency.

b, Mean ± s.e.m. cue-to-start latency distribution across rats (n = 14). Within each rat, latencies were binned on a logarithmic scale and converted to the proportion of trials in each bin; bin-wise proportions were then averaged across rats. After R1 outcomes, cue-to-start latency distributions showed a sharp early peak at approximately 500 ms with a long tail, indicating rapid cue-triggered initiation on a subset of trials.

c, Cue-to-start latency comparisons across rats (n = 14). *Left*, proportion of short-latency trials (< 1 s). *Middle*, median latency of short-latency trials (< 1 s). *Right*, median latency of long-latency trials (> 1 s). Short cue-to-start latencies occurred more frequently and were shorter on average after R1 than after R3/R5. Gray lines indicate paired data from individual rats. Statistical significance was determined using Wilcoxon signed-rank tests; *P < 0.05, ***P < 0.001; N.S., not significant.

d, Mean ± s.e.m. water-to-start latency distribution across rats (n = 14), analyzed as in **b**. The distributions of cue-to-start and water-to-start latencies differed. This finding supports the idea that initiation of the next trial is mediated by either cue-evoked re-engagement or spontaneous initiation following a reward, depending on the behavioral state at cue onset.

e, Mean ± s.e.m. trial-start latency distribution across rats (n = 14), analyzed as in **b**. For each trial, the trial-start latency was defined as the shorter of the cue-to-start and water-to-start latencies.

In **b**, **d**, and **e**, asterisks denote bins with significant differences between conditions (Wilcoxon signed-rank tests with Bonferroni correction across 10 bins; *P < 0.05, **P < 0.01).

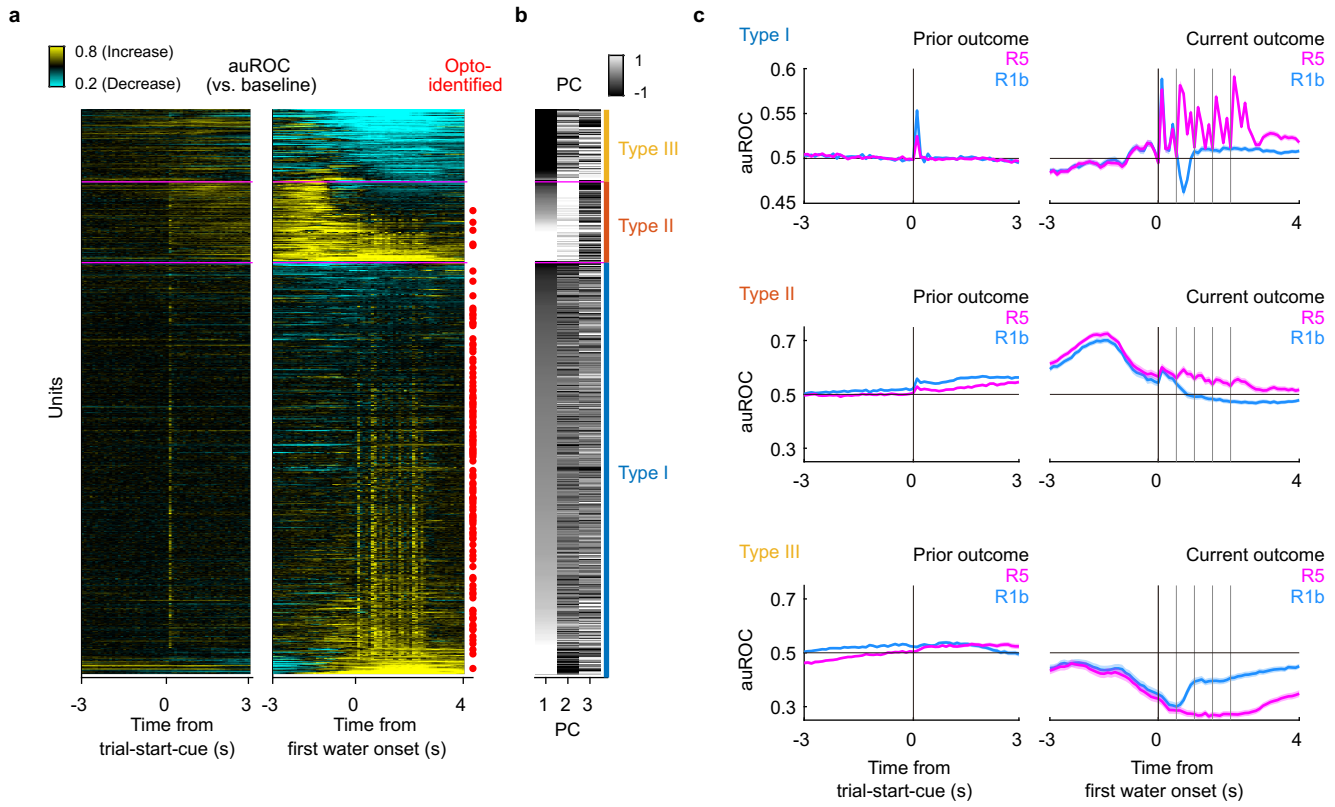

Supplementary Fig. 2 | Clustering of VTA unit activity.

a, Normalized activity shown as auROC values relative to pre-trial-start-cue activity (pre-L0; −3 to 0 s from L0 onset) for all recorded units (n = 780). Activity is aligned to the trial-start-cue onset for trials preceded by an R1b outcome (*left*) and to the water onset for trials with a current R5 outcome (*right*). For each unit, binned spike activity aligned to the trial-start-cue onset (−3 to 3 s) in trials following an R1b outcome and to water onset (−3 to 4 s) in R5 trials was concatenated, and auROC was computed relative to the pre-L0 window. Units were categorized into three clusters via k-means clustering based on their scores on the first three principal components (PC1–PC3; ~83% explained variance). These clusters correspond to phasic, positive-ramping (increasing activity), and negative-ramping (decreasing activity) units (Types I–III; n = 573, 117, and 90, respectively). Units were reordered by PC1 within each cluster. Optogenetically identified dopamine neurons (red dots) were predominantly categorized as Type I (111 of 115; 96.5%) and exhibited phasic responses to both trial-start-cue and water onset.

b, Projections (PC scores) of individual units onto PC1–PC3 used for clustering, ordered as in **a** and color-coded by cluster identity (Types I–III).

c, Mean ± s.e.m. auROC time courses of the three unit types aligned to trial-start-cue (*left*) and water onset (*right*), grouped by prior reward size (specifically, the reward delivered immediately before trial-start-cue onset; R1b versus R5; *left*) and current reward size (R1b versus R5; *right*). Light gray vertical lines in the *right* panels indicate the timings of the five consecutive water deliveries in R5 trials. For clarity, R1b and R5 are shown; similar subtype-specific temporal profiles were also observed for R1s and R3. In some traces, s.e.m. is smaller than the line width and therefore not visually discernible. auROC, area under the receiver operating characteristic curve.

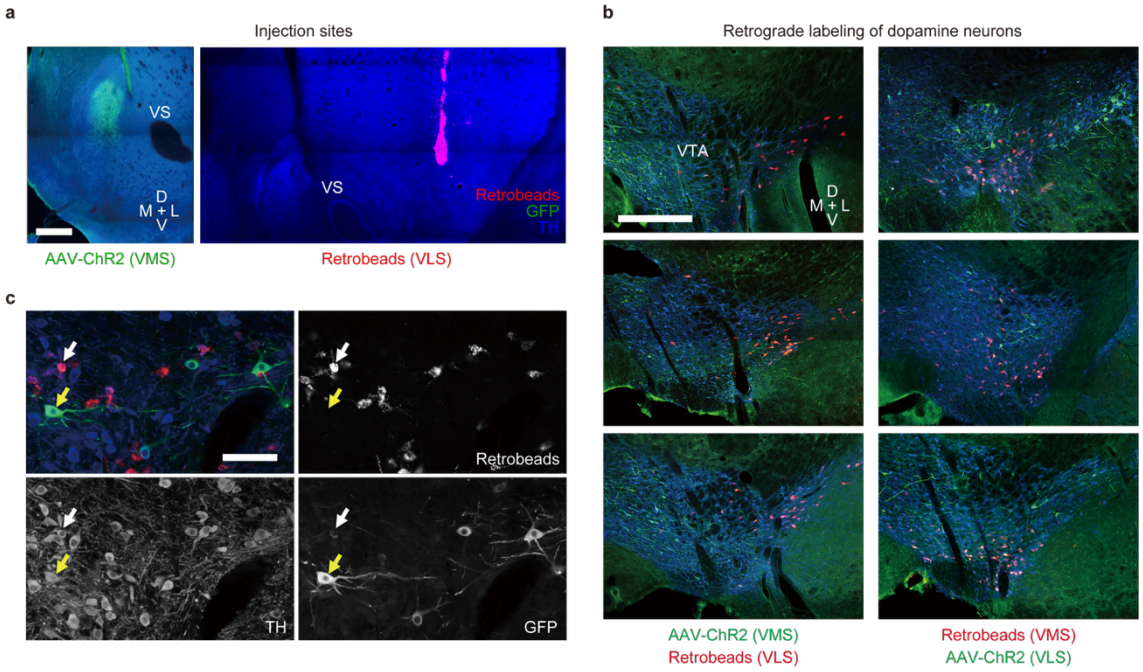

Supplementary Fig. 3 | Projection-specific labeling of VTA dopamine neurons.

a, Photomicrographs of representative injection sites in the ventral striatum (VS) of a TH-Cre rat. AAVrg-DIO-ChR2-EYFP was injected into the ventromedial striatum (VMS; *left*, green), and RetroBeads were injected into the ventrolateral striatum (VLS; *right*, red). TH immunostaining is displayed in blue. Scale bar, 500 µm.

b, Retrogradely labeled dopamine neurons in the VTA following injections of RetroBeads (red) into the VLS and AAVrg-DIO-ChR2-EYFP (green) into the VMS (*left column*, $n = 3$ rats), or RetroBeads into the VMS and AAVrg-DIO-ChR2-EYFP into the VLS (*right column*, $n = 3$ rats). TH immunostaining is displayed in blue. The *top-left* panel corresponds to the injection example shown in **a**. Labeled VTA neurons were localized more medially for VMS-projecting neurons and more laterally for VLS-projecting neurons. These distributions partially overlap, consistent with previous reports (de Jong et al. 2024[1] and Farassat et al. 2019[2]). Scale bar, 500 µm.

c, High-magnification micrographs of the lateral VTA showing overlapping signals of RetroBeads, GFP, and TH. VMS- and VLS-projecting dopamine neurons intermingled within the lateral VTA, particularly in the spatially overlapping regions shown in **b**. White arrows indicate TH-positive neurons labeled with RetroBeads (VMS-projecting), and yellow arrows indicate TH-positive neurons labeled with GFP (VLS-projecting). Scale bar, 100 µm.

D, dorsal; V, ventral; M, medial; L, lateral; VMS, ventromedial striatum; VLS, ventrolateral striatum; VTA, ventral tegmental area.

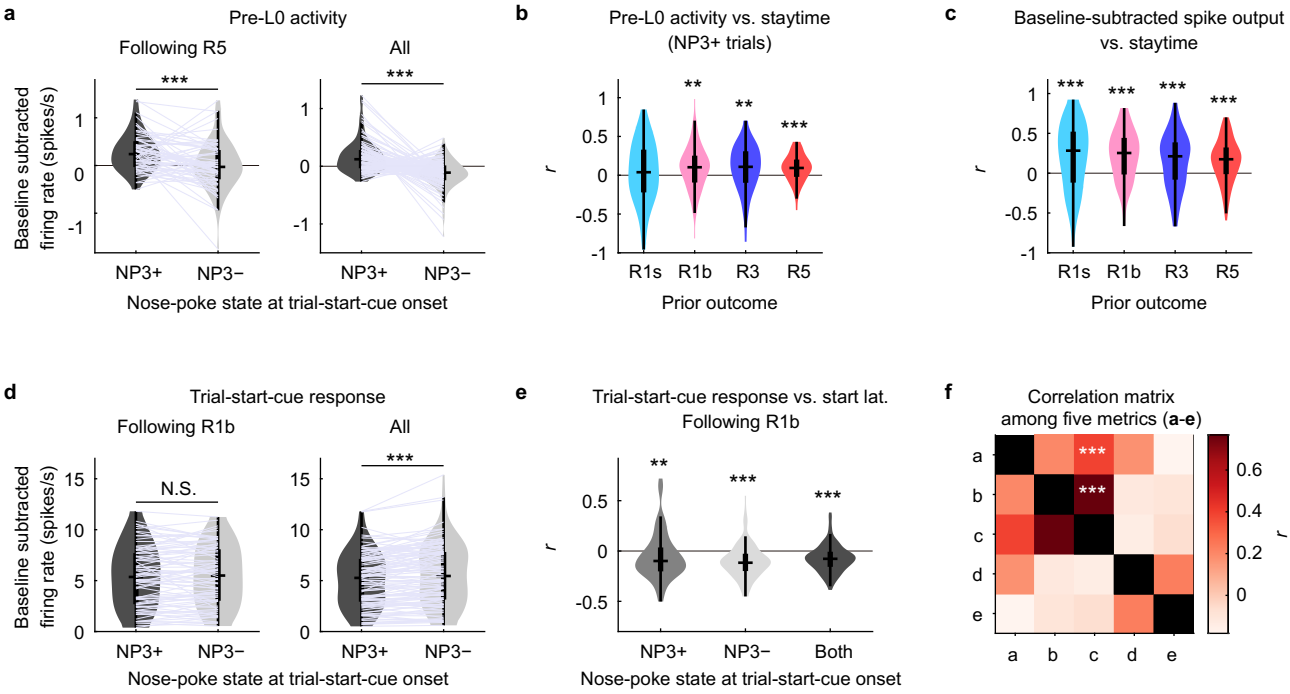

Supplementary Fig. 4 | Robustness of pre-L0 activity and trial-start-cue responses in analyses separated by nose-poke state.

Baseline and response definitions varied across panels: **a** and **b** use pre-L0 activity relative to trial-start-cue onset, **c** uses a pre-exit reference baseline relative to NP3-out to isolate activity during staytime, and **d** and **e** use trial-start-cue responses relative to trial-start-cue onset. To test whether dopamine–behavior relationships depended on overt nose-poke state at trial-start-cue onset, trials were separated into NP3+ trials, in which rats were still nose-poking in the water port, and NP3− trials, in which rats had already exited the water port. This distinction also corresponded to the latency component contributing to the integrated trial-start latency measure: in NP3+ trials, trial-start latency was determined by water-to-start latency, whereas in NP3− trials, it was determined by cue-to-start latency.

a, Pre-L0 activity preceding trial-start-cue onset (−4 to 0 s) compared between NP3+ and NP3− trials. Pre-L0 activity was quantified as a baseline-subtracted firing rate, computed as the firing rate in the −4 to 0 s window minus the mean firing rate in the same window across all trials. *Left*, analysis restricted to trials with prior outcome R5 (n = 67 units). *Right*, the same analysis with all rewarded trials from all optogenetically identified VTA dopamine neurons pooled together (n = 115 units). Pre-L0 activity was significantly higher in NP3+ than in NP3− trials in both analyses (Wilcoxon signed-rank tests; ***$P < 0.001$). Units were included if both nose-poke states contained more than five trials.

b, Pearson's r values for correlations between pre-L0 activity and staytime in NP3+ trials, separated by prior outcome (the reward delivered immediately before trial-start-cue onset; R1s, R1b, R3, R5). Correlations were tested against zero using Wilcoxon signed-rank tests with Bonferroni correction across four comparisons (n = 77, 86, 105, and 115 units, respectively; **$P < 0.01$, ***$P < 0.001$). Units were included if the number of trials contributing to a given correlation exceeded five. Positive correlations within NP3+ trials indicate that the pre-L0 activity–staytime relationship persisted within a fixed nose-poke state.

c, Supplementary analysis of activity during staytime. Pearson's r values were computed for

correlations between baseline-subtracted spike output during staytime and staytime duration during water-port engagement, stratified by prior outcome as in **b**. Spike output was computed over the staytime period after excluding the water delivery window [0.5 s for single-drop rewards (R1s/R1b), 1.5 s for R3, and 2.5 s for R5], thereby removing reward-evoked activity from the analysis window. For each trial, spike output was baseline-subtracted by removing the expected baseline spikes (mean baseline rate × adjusted staytime duration). Because mean firing rates gradually decreased during staytime toward the level observed near NP3-out, the reference baseline was defined as the 1-s period preceding NP3-out (−1 to 0 s). This baseline-subtracted output provides a cumulative measure of above-baseline activity during reward-site engagement (Zhu et al. 2025[3]; see Methods for details). Correlations were tested against zero using Wilcoxon signed-rank tests with Bonferroni correction across four comparisons (n = 108, 115, 107, and 115 units, respectively; ***$P < 0.001$). Units were included if the number of trials contributing to each correlation exceeded five.

d, Trial-start-cue responses (0 to 0.2 s after trial-start-cue onset) were compared between NP3+ and NP3− trials. *Left*, analysis restricted to trials with prior outcome R1b (n = 84 units). *Right*, analysis pooling all rewarded trials from all optogenetically identified VTA dopamine neurons (n = 115 units). No difference was observed after R1b, whereas a robust difference emerged in the pooled analysis (Wilcoxon signed-rank tests; N.S., not significant; ***$P < 0.001$). Units were included if both nose-poke states contained more than five trials. The absence of a difference after R1b indicates that trial-start-cue responses in the condition used for the main correlation analysis were not simply determined by overt nose-poke state.

e, Pearson's r values for correlations between trial-start-cue responses and trial-start latency, computed from NP3+ trials only, NP3− trials only, or both states combined (n = 86, 114, and 115 units, respectively). All three analyses showed significant negative correlations (Wilcoxon signed-rank tests; **$P < 0.01$, ***$P < 0.001$), indicating that cue-evoked responses tracked trial-start latency irrespective of overt nose-poke state at trial-start-cue onset. Units were included if both nose-poke states contained more than five trials.

f, Correlation matrix summarizing the relationships among neuron-specific metrics derived from **a–e** for all optogenetically identified VTA dopamine neurons (n = 115). Each metric was computed once per neuron using the trial set specified for the corresponding panel: (**a**) NP3+ versus NP3− pre-L0 activity differences from all rewarded trials; (**b**) pre-L0 activity–staytime correlations from NP3+ trials with prior outcome R5; (**c**) staytime–spike-output correlations during staytime from NP3+ trials with prior outcome R5; (**d**) NP3+ versus NP3− trial-start-cue response differences from all rewarded trials; and (**e**) trial-start-cue response–trial-start latency correlations from NP3+ and NP3− trials combined. Pearson's r values were calculated for each pair of metrics across neurons (10 pairs total). Only two pairs, (**a–c**) and (**b–c**), remained significant after Bonferroni correction (***$P < 0.001$), indicating that metrics related to pre-L0 activity and staytime covaried across neurons, whereas trial-start-cue-related metrics showed weaker relationships with these measures. Because the matrix is symmetric, significance markers are shown only for the 10 unique pairs in the upper triangle.

Light gray lines in **a** and **d** connect paired values from the same neuron. Together, these analyses indicate that the relationships between pre-L0 activity and staytime, and between trial-start-cue responses and trial-start latency, were not explained solely by nose-poke state at trial-start-cue onset or by the latency component contributing to the integrated trial-start latency measure.

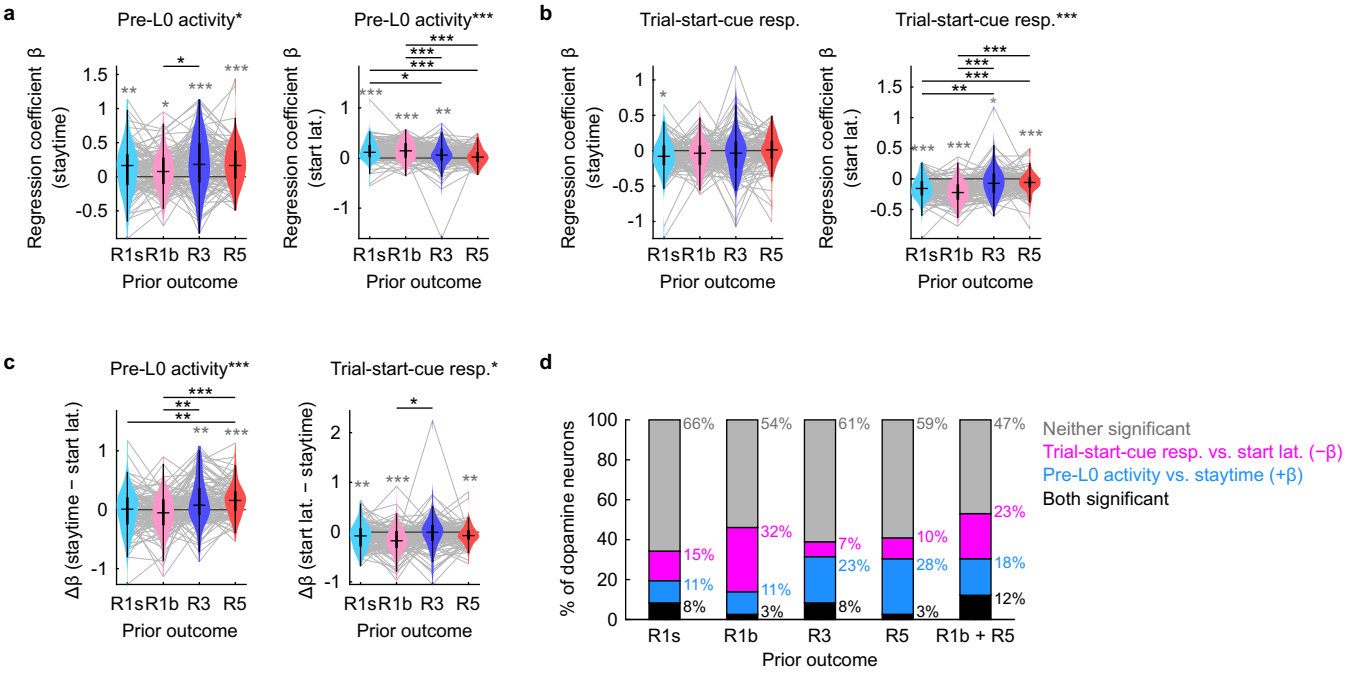

Supplementary Fig. 5 | Regression coefficients characterizing the relationships between dopamine neuron activity and behavioral variables across prior outcomes.

a, Regression coefficients (β) predicting z-scored pre-L0 activity (−4 to 0 s before trial-start-cue onset) from z-scored staytime (*left*) or z-scored log-transformed trial-start latency (*right*). Coefficients were estimated independently for each prior outcome (R1s, R1b, R3, and R5). Pre-L0 activity showed significantly positive regression coefficients for staytime across all prior outcomes. Regression models were fitted separately for each optogenetically identified dopamine neuron recorded in both SMALL and BIG blocks (n = 108), using pooled trials across block types and including the session-level z-scored trial number as an additional covariate.

b, Same as **a** but for regression coefficients predicting z-scored trial-start-cue responses (0 to 0.2 s after cue onset). Trial-start-cue responses showed more negative regression coefficients for trial-start latency after small rewards (R1s and R1b) than after large rewards (R3 and R5).

c, Contrasts in regression coefficients ($\Delta\beta$) summarizing the relative contributions of staytime and trial-start latency to pre-L0 activity and trial-start-cue responses across prior outcomes. For pre-L0 activity (*left*), $\Delta\beta = \beta_{\text{staytime}} - \beta_{\text{start lat.}}$, such that positive values indicate a more positive, or less negative, coefficient for staytime than for trial-start latency. For trial-start-cue responses (*right*), $\Delta\beta = \beta_{\text{start lat.}} - \beta_{\text{staytime}}$, such that positive values indicate a more positive, or less negative, coefficient for trial-start latency than for staytime. Shifts in $\Delta\beta$ across prior outcomes quantify how the dominant behavioral predictor changes with reward size.

d, Proportions of dopamine neurons meeting two significance criteria across prior outcomes: a significantly negative regression coefficient for trial-start-cue responses versus trial-start latency and a significantly positive regression coefficient for pre-L0 activity versus staytime. Neurons showing both patterns are indicated in black, and neurons showing neither pattern are indicated in gray. The final column (R1b + R5) summarizes the classification using the negative trial-start-latency-related coefficient from R1b and the positive staytime-related coefficient from R5. Numerals indicate the

percentage of neurons in each category.

For **a–c**, asterisks in the panel titles indicate significant effects of prior outcome in Friedman tests across the four reward conditions (*P < 0.05, ***P < 0.001). Asterisks above horizontal brackets indicate significant post hoc Tukey–Kramer tests between specific reward conditions (*P < 0.05, **P < 0.01, ***P < 0.001), and asterisks directly above the individual distributions indicate significant deviations of the regression coefficients from zero (Wilcoxon signed-rank tests with Bonferroni correction across the four prior outcomes; *P < 0.05, **P < 0.01, ***P < 0.001). For all panels, the prior outcome was defined as the reward delivered immediately before the end of the latency interval (staytime or trial-start latency) or immediately before the duration during which pre-L0 activity or trial-start-cue responses were calculated.

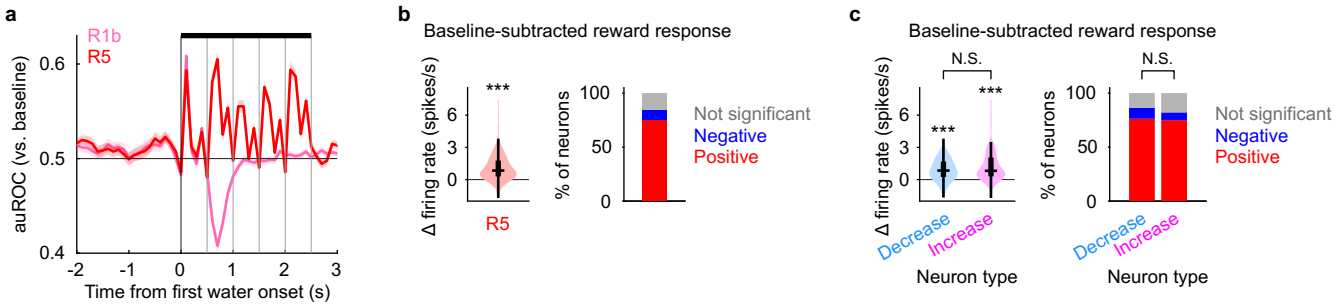

Supplementary Fig. 6 | Reward responses are comparable between increase- and decrease-type dopamine neurons.

a, Mean ± s.e.m. normalized activity (auROC relative to the firing rate in the pre-trial-start-cue window, −1 to 0 s from trial-start-cue (L0) onset; 100-ms bins) of optogenetically identified dopamine neurons (n = 115) aligned to water onset (first drop) in trials with five sequentially delivered rewards (R5, red) or a single reward (R1b, pink). Gray vertical lines indicate water-delivery timings in R5 trials; the black bar denotes the reward-response window used in **b** and **c**.

b, Baseline-subtracted reward response in R5 trials. Pre-L0 firing rate was defined for each neuron as the mean firing rate in the pre-trial-start-cue window (−1 to 0 s from trial-start-cue (L0) onset), averaged across all trials. For each R5 trial, the baseline-subtracted reward response was computed as the mean firing rate in the reward window (0 to 2.5 s after water onset; black bar in **a**) minus this pre-L0 firing rate. *Left*, baseline-subtracted reward responses across neurons (Wilcoxon signed-rank test against zero, ***$P < 0.001$). *Right*, proportions of neurons displaying significantly positive (red) or negative (blue) reward responses. For each neuron, trial-wise baseline-subtracted reward responses were evaluated against zero across trials (Wilcoxon signed-rank test, $P < 0.05$); the remaining neuronal population was categorized as not significantly modulated (gray).

c, Comparison of baseline-subtracted R5 reward responses between decrease-type (n = 59) and increase-type (n = 56) dopamine neurons. *Left*, baseline-subtracted reward responses in each subtype; asterisks above each distribution denote significant excitation relative to zero (Wilcoxon signed-rank test, ***$P < 0.001$), and "N.S." above the horizontal bracket indicates no significant difference between subtypes (Wilcoxon rank-sum test, $P > 0.05$). *Right*, proportions of neurons in each subtype showing significantly positive (red) or negative (blue) reward responses, or no significant modulation, using the same within-neuron criterion as in **b** (Wilcoxon signed-rank test against zero, $P < 0.05$). Population differences in the proportions of neurons with positive, negative, or nonsignificant reward responses between subtypes were evaluated with a χ^2 test ("N.S.", $P > 0.05$).

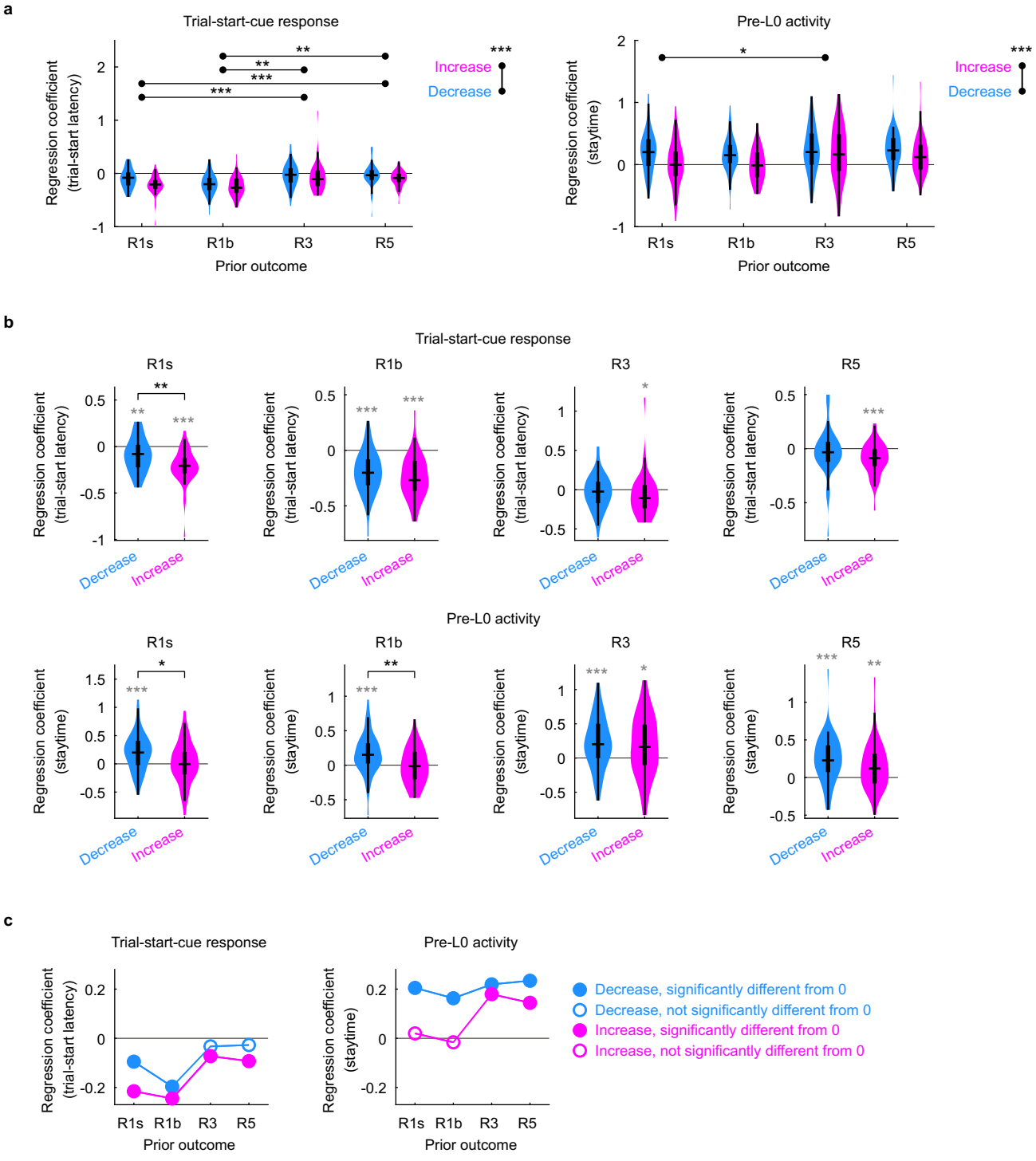

Supplementary Fig. 7 | Regression coefficients for predicting pre-L0 activity and trial-start-cue responses, separated by dopamine neuron subtype.

a, Regression coefficients were derived from the same multiple linear regression models used in **Supplementary Fig. 5,** shown separately by dopamine neuron subtype (decrease-type, n = 59; increase-type, n = 56) and prior outcome (R1s, R1b, R3, R5). *Left*, regression coefficients predicting z-scored trial-start-cue responses (0 to 0.2 s after trial-start-cue onset; "Trial-start-cue response") from

z-scored trial-start latency ("Regression coefficient (trial-start latency)"). *Right*, regression coefficients predicting z-scored pre-L0 activity (−4 to 0 s before trial-start-cue onset; "Pre-L0 activity") from z-scored staytime ("Regression coefficient (staytime)"). Increase-type neurons displayed more negative coefficients for predicting trial-start-cue responses from trial-start latency, whereas decrease-type neurons showed more positive coefficients for predicting pre-L0 activity from staytime. Statistical analysis was performed with a two-way ANOVA (independent variables: dopamine subtype and prior outcome), followed by Tukey–Kramer post hoc tests when main effects were significant (*$P < 0.05$, **$P < 0.01$, ***$P < 0.001$).

b, The same regression coefficients as in **a**, replotted separately for each prior outcome to compare increase- and decrease-type neurons within each condition. *Top*, regression coefficients predicting trial-start-cue responses from trial-start latency. *Bottom*, regression coefficients predicting pre-L0 activity from staytime. For each outcome, regression coefficients for increase- and decrease-type neurons were compared using Wilcoxon rank-sum tests and tested against zero within each subtype using Wilcoxon signed-rank tests with Bonferroni correction across the two within-subtype tests (*$P < 0.05$, **$P < 0.01$, ***$P < 0.001$).

c, Summary plots showing the mean regression coefficients across prior outcomes for increase- and decrease-type neurons. For each outcome and subtype, the regression coefficients were tested against zero using the same Wilcoxon signed-rank tests as in **b**. Filled circles indicate coefficients significantly different from zero after Bonferroni correction ($P < 0.05$); open circles indicate nonsignificant coefficients.

For all panels, the prior outcome was defined as the reward delivered immediately before the end of the latency interval (staytime or trial-start latency) or immediately before the duration during which pre-L0 activity or trial-start-cue responses were calculated.

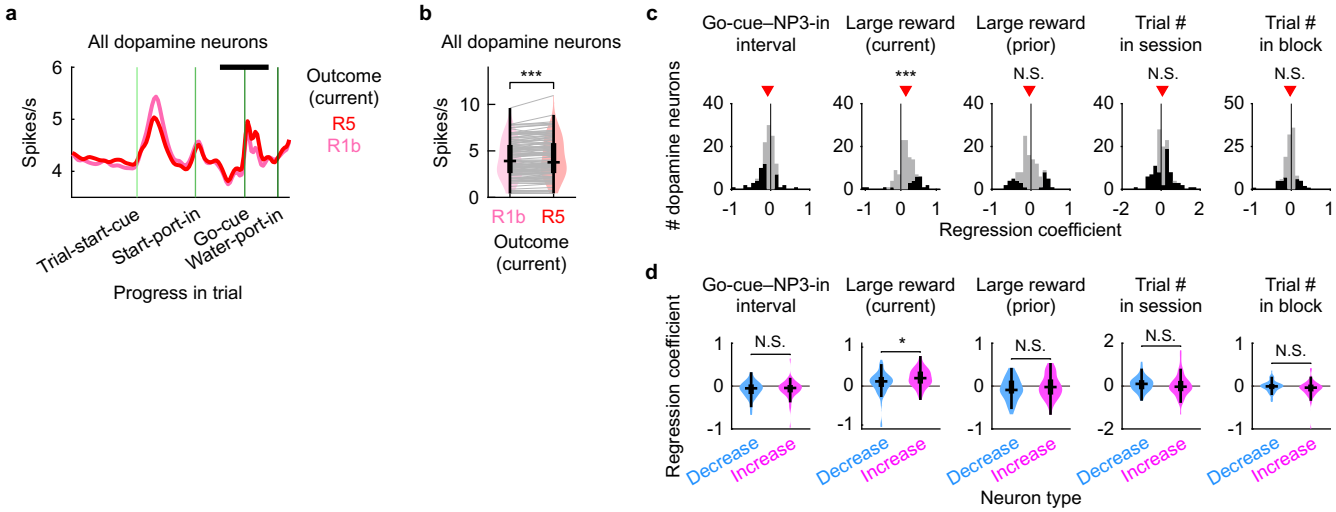

Supplementary Fig. 8 | Dopamine neurons encode predicted upcoming reward size during the period around the go-cue.

Related to **Fig. 7**, this analysis examines whether the encoding of predicted upcoming reward size during the go-cue period persists when prior-trial reward size is included as an additional covariate in a regression model.

a, Time-in-trial-aligned activity showing the mean firing rates of all optogenetically identified dopamine neurons ($n = 115$) during large-reward (R5, red) and small-reward (R1b, pink) trials in BIG blocks, with trials pooled across prior outcomes. Vertical lines indicate task events (trial-start-cue, start-port-in, go-cue, and water-port-in). The black bar denotes the go-cue-centered analysis window (−1.5 to 1.5 s from go-cue onset in real, unwarped time) used in **b**–**d**.

b, Mean firing rates during the go-cue window (black bar in **a**), comparing R1b and R5 trials across the dopamine neuron population (BIG-block trials only; Wilcoxon signed-rank test; ***$P < 0.001$).

c, Distributions of regression coefficients across dopamine neurons ($n = 115$) from multiple linear regression models fitted separately for each neuron to predict trial-by-trial dopamine responses (z-scored firing rates in the go-cue window). Predictors included the z-scored interval from go-cue onset to water-port-in (NP3-in) ("Go-cue–NP3-in interval"); upcoming reward size on the current trial ("Large reward (current)"; binary indicator: 1 = R5, 0 = R1b); reward size on the immediately preceding trial ("Large reward (prior)"; binary indicator: 1 = R5, 0 = R1b); z-scored trial number within session ("Trial # in session"); and z-scored trial number within block ("Trial # in block"). Only BIG-block trials were included. Black bars denote neurons with significant coefficients for the corresponding predictor ($P < 0.05$; t-test of the regression coefficient); light gray bars denote neurons with nonsignificant coefficients. Red arrowheads denote the mean regression coefficient across neurons; population-level deviations from zero were evaluated using Wilcoxon signed-rank tests (***$P < 0.001$; N.S., $P > 0.05$).

d, The same regression coefficients as in **c**, separated by dopamine neuron type (increase-type, $n = 56$; decrease-type, $n = 59$). Regression coefficients were compared between neuron types using Wilcoxon rank-sum tests (*$P < 0.05$; N.S., $P > 0.05$).

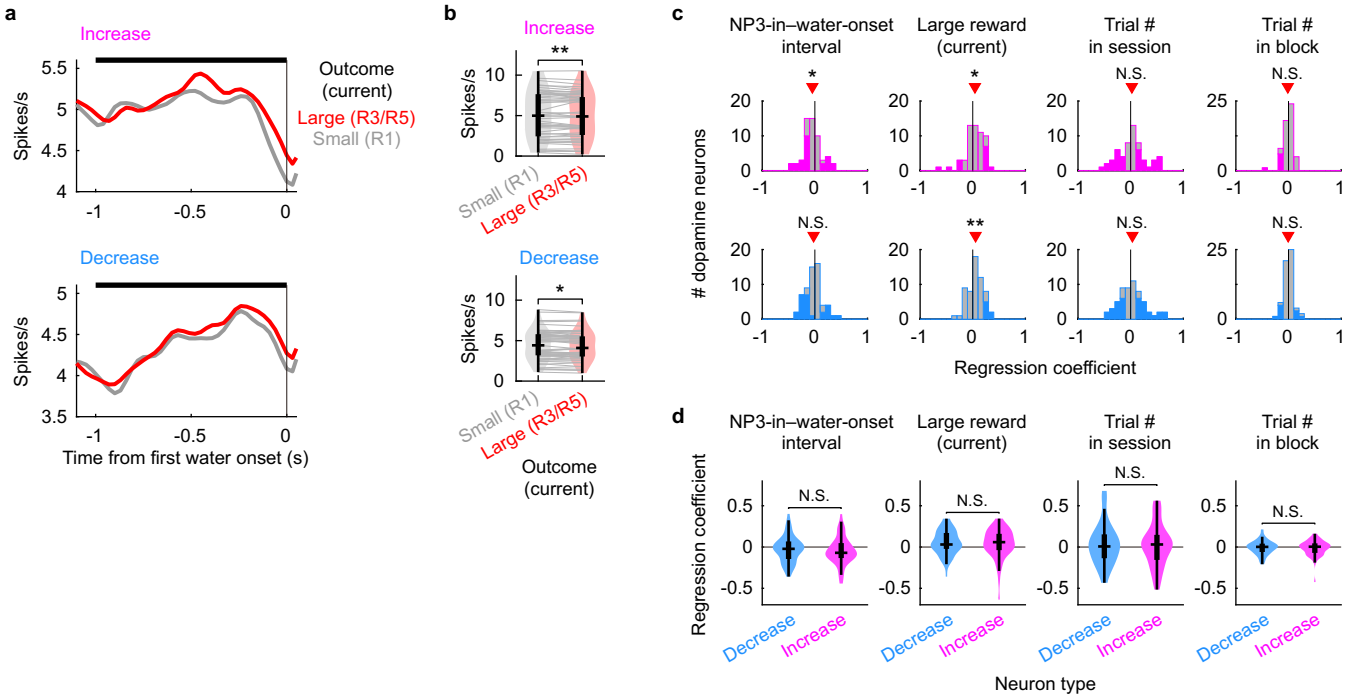

Supplementary Fig. 9 | Pre-water-onset activity in both dopamine neuron types is modulated by upcoming reward size.

a, PSTHs showing mean firing rates of increase-type (*top*; $n = 51$) and decrease-type (*bottom*; $n = 57$) dopamine neurons aligned to water onset (−1.2 to 0.1 s). Trials with current large-reward (R3/R5, red) and small-reward (R1, gray) are compared. Panels **a** and **b** utilize the subset of optogenetically identified dopamine neurons recorded in both SMALL and BIG blocks ($n = 108$).

b, Mean firing rates during the pre-reward window (−1 to 0 s; black bar in **a**) were evaluated across current small- and large-reward trials for increase-type (*top*) and decrease-type (*bottom*) neurons (using the same neurons as in **a**) (Wilcoxon signed-rank test; $^*P < 0.05$, $^{**}P < 0.01$).

c, Distributions of regression coefficients from per-neuron multiple linear regression models predicting trial-by-trial z-scored firing rates during the same pre-reward window (−1 to 0 s) using four predictors: the duration from the first water-port-in (NP3-in) to the first water onset ("NP3-in–water-onset interval"), which varied across trials depending on the time required to satisfy the NP3 hold requirement; reward size on the current trial ("Large reward (current)"; binary indicator: 1 = R3/R5, 0 = R1); trial number within session ("Trial # in session"); and trial number within block ("Trial # in block"). Trials from both BIG and SMALL blocks were included. This analysis utilizes the same regression framework as in **Fig. 7**, with the NP3-in–water-onset interval as the timing covariate. Panels **c** and **d** use the full set of optogenetically identified dopamine neurons ($n = 115$). Coefficients are shown separately for increase-type (*top*; $n = 56$) and decrease-type (*bottom*; $n = 59$) neurons. Colored bars denote neurons with significant regression coefficients (t-test of the regression coefficient; $P < 0.05$); light gray bars denote neurons with nonsignificant coefficients. Red arrowheads denote the mean regression coefficient across neurons; population-level deviations from zero were evaluated using Wilcoxon signed-rank tests ($^*P < 0.05$, $^{**}P < 0.01$; N.S., $P > 0.05$).

d, Regression coefficients for each predictor are shown separately for increase- and decrease-type neurons (Wilcoxon rank-sum tests; N.S., $P > 0.05$).

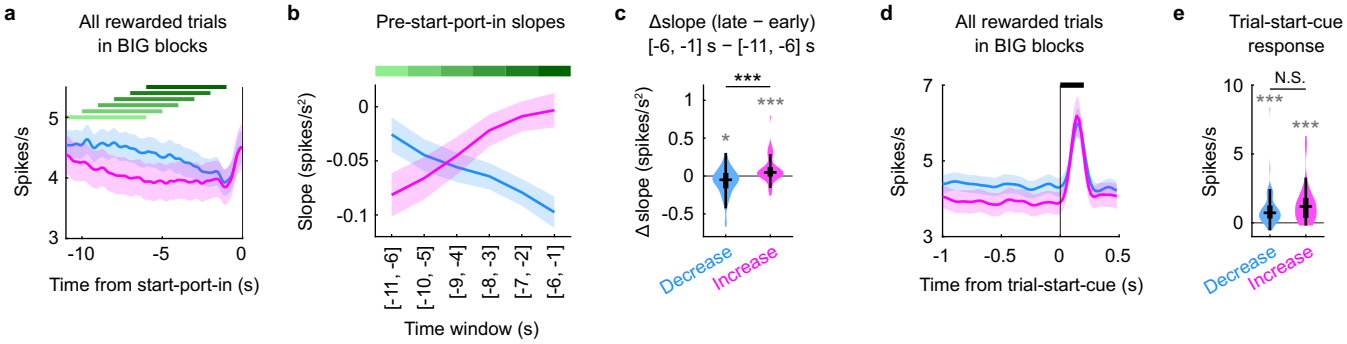

Supplementary Fig. 10 | Pre-initiation activity transitions in increase- and decrease-type dopamine neurons.

a, Mean firing rates (mean ± s.e.m.) of increase-type (magenta; $n = 56$) and decrease-type (cyan; $n = 59$) dopamine neurons aligned to start-port-in (NP0-in). All rewarded trials from BIG blocks were included (not separated by prior outcome).

b, Pre-start-port-in slopes (mean ± s.e.m.) computed in overlapping 5-s windows sliding in 1-s steps, using the same neurons as in **a** (windows: −11 to −6, −10 to −5, −9 to −4, −8 to −3, −7 to −2, and −6 to −1 s; green bars in **a**). For each neuron and each window, a linear regression was fitted to the firing rate within the 5-s window to derive a slope; slopes were then averaged across neurons within each subtype (see Methods). Increase- and decrease-type neurons demonstrated opposing dynamics in these pre-start-port-in slopes.

c, Late–early slope differences of the neurons shown in **a**. For each neuron, an early slope was defined from −11 to −6 s and a late slope from −6 to −1 s; the difference was computed as (late − early). Differences were evaluated between neuron types (black asterisks, Wilcoxon rank-sum test) and relative to zero within each type (gray asterisks, Wilcoxon signed-rank test). Within-type tests were Bonferroni-corrected ($n = 2$) (*$P < 0.05$, ***$P < 0.001$; N.S., $P > 0.05$).

d, Mean firing rates (mean ± s.e.m.) of increase- and decrease-type neurons aligned to the trial-start-cue, utilizing the same BIG-block rewarded trials and neurons as in **a**.

e, Baseline-subtracted trial-start-cue-evoked responses (0 to 0.2 s after cue onset; black bar in **d**) for the same neurons as in **a**. For each neuron, responses were computed as firing rate in the response window minus the mean pre-cue firing rate of that neuron (−1 to 0 s relative to trial-start-cue onset), averaged across BIG-block rewarded trials. Responses were evaluated across neuron types (black asterisks, Wilcoxon rank-sum test) and relative to zero within each type (gray asterisks, Wilcoxon signed-rank test). Within-type tests were Bonferroni-corrected ($n = 2$) (*$P < 0.05$, ***$P < 0.001$; N.S., $P > 0.05$).

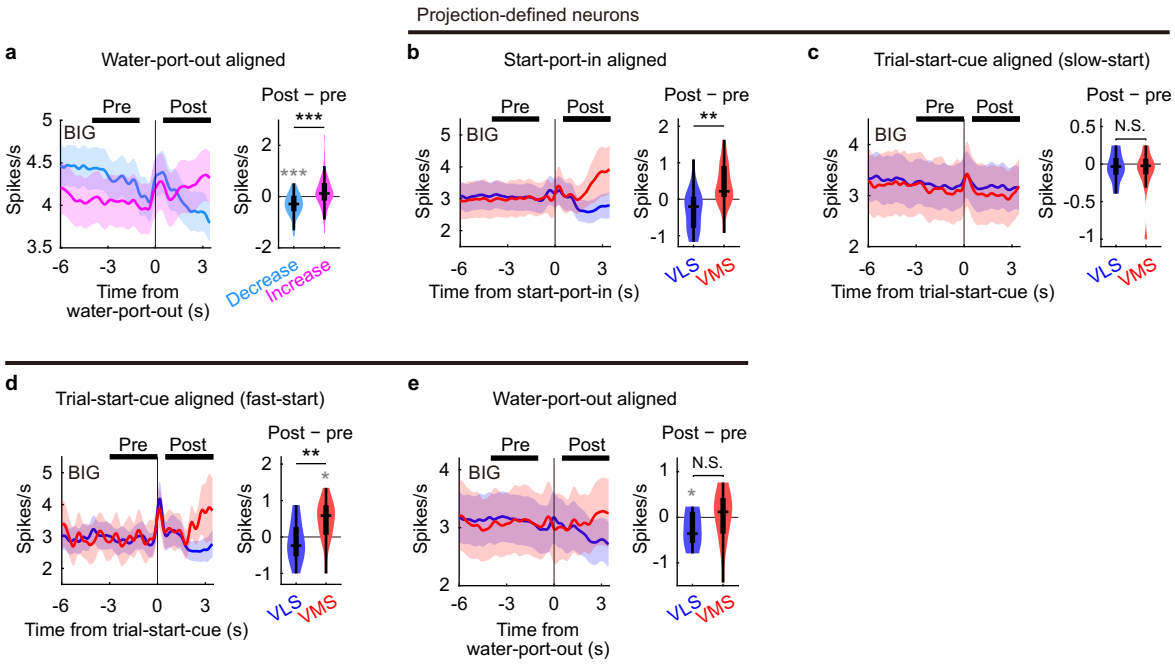

Supplementary Fig. 11 | Activity transitions around behavioral transition points across dopamine neuron subtypes and projection groups.

a, Activity of increase- and decrease-type dopamine neurons aligned to water-port-out in BIG blocks. *Left*, mean ± s.e.m. firing rates of increase-type ($n = 56$) and decrease-type ($n = 59$) dopamine neurons aligned to water-port-out. *Right*, changes in firing rate quantified as Post minus Pre. Post and Pre windows were 0.5–3.5 s and −4 to −1 s from water-port-out, respectively.

b–e, Activity of projection-defined VMS- and VLS-projecting dopamine neurons in BIG blocks aligned to start-port-in (**b**), to trial-start-cue onset in slow-start trials (**c**; cue-to-start latency > 1 s), to trial-start-cue onset in fast-start trials (**d**; cue-to-start latency < 1 s), and to water-port-out (**e**). *Left*, mean ± s.e.m. firing rates of VMS-projecting ($n = 14$) and VLS-projecting ($n = 21$) dopamine neurons. *Right*, changes in firing rate quantified as Post minus Pre. Post windows were 0.5–3.5 s from start-port-in (**b**), trial-start-cue onset (**c,d**), or water-port-out (**e**). Pre windows were −4 to −1 s from start-port-in (**b**), −3 to 0 s from trial-start-cue onset (**c,d**), or −4 to −1 s from water-port-out (**e**).

Post–Pre values were compared between projection groups (black; Wilcoxon rank-sum tests; $***P < 0.001$, $**P < 0.01$; N.S., $P > 0.05$) and against zero within each group (gray; Wilcoxon signed-rank tests; $***P < 0.001$, $*P < 0.05$; nonsignificant comparisons not shown). Within-group tests were Bonferroni-corrected ($n = 2$).

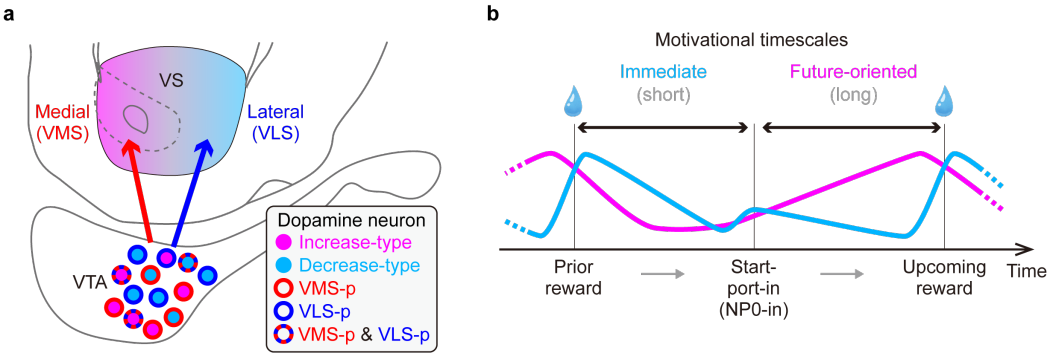

Supplementary Fig. 12 | Schematic summary of projection-biased dopamine neuron subpopulations associated with current reward engagement and next-trial initiation.

a, Schematic illustrating projection-biased midbrain dopamine neuron subpopulations in the VTA and their preferential projections to medial and lateral ventral striatal regions. Magenta and cyan denote increase- and decrease-type dopamine neurons, respectively. Solid red and blue outlines of schematic dopamine neurons denote VMS-projecting (VMS-p) and VLS-projecting (VLS-p) neurons, respectively, whereas dashed red-and-blue outlines denote neurons projecting to both regions. Red and blue arrows denote projections toward medial and lateral ventral striatal regions, respectively. The medial and lateral VS regions schematically represent VMS- and VLS-biased projection territories, respectively. The color gradient indicates partial overlap between these territories. The cyan-to-magenta gradient indicates that decrease- and increase-type dopamine neuron subpopulations show partially overlapping but lateral- and medial-biased projections, respectively.

b, Conceptual diagram illustrating the distinct motivational timescales associated with the two dopamine response types. Increase-type neurons (magenta) are biased toward signals associated with preparation for the subsequent reward opportunity. Decrease-type neurons (cyan) are biased toward engaging with the current reward. The schematic illustrates the behavioral transition from engagement with the current reward after the prior reward to the start-port-in (NP0-in), which signifies commitment to the next trial, followed by an approach toward the upcoming reward.

VTA, ventral tegmental area; VS, ventral striatum; VMS, ventromedial striatum; VLS, ventrolateral striatum.

References

1. de Jong, J. W., Liang, Y., Verharen, J. P. H., Fraser, K. M. & Lammel, S. State and rate-of-change encoding in parallel mesoaccumbal dopamine pathways. *Nat. Neurosci.* **27**, 309–318 (2024). https://doi.org/10.1038/s41593-023-01547-6.
2. Farassat, N. *et al.* In vivo functional diversity of midbrain dopamine neurons within identified axonal projections. *eLife* **8**, e48408 (2019). https://doi.org/10.7554/eLife.48408.
3. Zhu, Z. *et al.* Hedonic eating is controlled by dopamine neurons that oppose GLP-1R satiety. *Science* **387**, eadt0773 (2025). https://doi.org/10.1126/science.adt0773.